A computational study on the drag reduction effectiveness of a spinning projectile with different afterbody configurations at supersonic speeds

Quang Tuan Nguyen

Le Quy Don Technical University, Faculty of Special Equipment, Hanoi, Socialist Republic of Vietnam

e-mail: tuannguyenmta28@gmail.com, **corresponding author**,
ORCID iD: https://orcid.org/0000-0002-7741-8232

https://doi.org/10.5937/vojtehg73-57712

FIELD: mechanical engineering, fluid dynamics, exterior ballistics
ARTICLE TYPE: original scientific paper

Abstract:

Introduction/purpose: In this paper, five Army-Navy Spinner Rocket configurations with different afterbodies were numerically evaluated on drag reduction effectiveness at supersonic speeds.

Methods: Reynolds-Averaged Navier-Stokes equations with the SST k-ω turbulence model were employed for numerical simulations. Mesh sensitivity studies were undertaken to ensure the independence of simulation results on the mesh size. The simulation results were validated against archival experimental data. A comparison of aerodynamic drag coefficients for baseline and modified afterbodies was carried out. The flow fields around different afterbody configurations were visualized and analyzed.

Results: The research results have indicated that a conical boattail or a combination of a conical boattail with a base cavity are the most effective methods showing on the average 10.99% and 11.96% in drag reduction, respectively. The base cavity configuration alone is the least effective method showing an average drag reduction of only 1.33% compared to the baseline configuration. The multi-step afterbody configuration can come up with an average drag reduction of 2.15% compared to the baseline configuration.

Conclusion: Afterbody configurations significantly affect the aerodynamic drag of a spinning projectile. Out of the considered afterbody configurations, the combination of a conical boattail and a base cavity is the most effective way to reduce a projectile drag. The findings presented in this study have provided significant insights into better understanding of passive methods for aerodynamic drag reduction.

Key words: numerical simulation, aerodynamic characteristics, drag reduction, conical boattail, base cavity.

Introduction

Aerodynamic drag is a crucial factor affecting the performance of projectiles such as missiles, rockets, artillery shells, and bullets. Reducing aerodynamic drag not only improves the effectiveness and precision of projectiles but also enhances their operational efficiency by extending their range and reducing the energy required for propulsion. Over the past decades, a wide range of methods have been developed to reduce projectile aerodynamic drag, each method being suitable for specific types of projectiles and their operational conditions. There are several means applied to reduce total drag acting on projectiles during their flight. Among them, the most practical and effective method is to lower projectile base drag by using a conventional axisymmetric conical boattail afterbody and other unconventional afterbodies such as a triangular afterbody, a square afterbody, a multi-step afterbody or a base cavity, slot cavity afterbodies, etc.

In recent years, there is a renewed interest in drag reduction research for missiles and projectiles. Platou (1975) conducted a series of experiments with unconventional projectile boattails and concluded that these unconventional projectile boattails have improved aerodynamic performance over the standard conical boattail. These boattails have equal or lower drag and an improved gyroscopic stability. Mathur and Viswanath (2004) experimentally investigated the effect of square-based afterbodies at high speeds on drag and concluded that, compared to conventional axisymmetric boattails with conical and circular-arc profiles, square-based afterbodies have the lowest total drag in the Mach number range of 0.95–1.60. El-Awwad et al. (2020) have investigated the aerodynamic characteristics and ballistic performance of projectiles with a triangular base and came to the conclusion that the triangular boattial has a base drag reduction of approximately 5% at M > 1.0 compared to the conventional conical boattail with the same length and the angle of inclination; also, the triangular boattail projectile has better performance from the stability point of view. The studies on the effectiveness of base cavities, ventilated cavities, locked vortex afterbodies, and multi-step afterbodies by Viswanath and Patil (1997) have indicated that base drag and total drag have been significantly reduced with unconventional boattail configurations. Lunghi et al. (2024) investigated the potential of multiple grooves to lower the aerodynamic drag on a boat-tailed bluff body. The work has revealed that the presence of two consecutive transverse grooves results in a maximum boat-tail drag reduction of 23.2%. Ibrahim and Filipone (2010) performed experimental and computational studies on the effect of streamwise slots applied to the

boattail on the total drag coefficient. Guidos and Sturek (1987) conducted a study on the aerodynamics of a 25mm diameter practice round with a triangular afterbody using a thin-layer Parabolized Navier-Stokes computational technique. Kumar et al. (2014) numerically studied the flow around a conical nose with a rounded tail projectile of 120mm caliber at three flow regimes and stated that the rounded tail is a better option than the boattail in terms of drag reduction. Lu and Zhang (2022) investigated the effect of the base cavity shape and dimensions on drag reduction of a slender body. Viswanath (2001) performed an investigation to analyse the aerodynamics of the flow around a multi-step afterbody and compared the drag of multi-step afterbodies with that of the blunt afterbody. The obtained result showed that the multi-step afterbody has smaller total drag than the baseline model. Viswanath and Patil (1990) conducted an experimental investigation into the effect of several base modifications, namely, base cavities, ventilated cavities, and two vortex suppression devices, on the reduction of total drag and base drag. The main conclusion drawn from his work is that, while several devices can provide appreciable base drag reduction, the net total drag reduction is relatively lower, possibly due to additional losses related to the devices. Fu and Liang (1994) carried out a numerical study on optimal drag reduction for a spinning projectile at transonic speeds with a passive control device. Mariotti et al. (2017) conducted numerical and experimental investigations to assess the efficiency and performance of a control method to delay boundary layer separation consisting of the introduction on the surface of contoured transverse grooves. Mahdi and Al-Atabi (2008) predicted the impact of forebody and afterbody geometries on the aerodynamic performance of several projectile bodies at supersonic speeds using analytical methods. The results of this work have shown that the lowest drag was obtained with a cone-cylinder configuration for the forebody and drag can be reduced by boattailing the afterbody. Ma et al. (2020) carried out a comparative study of the aerodynamic characteristics of a spinning projectile with cylindrical and boattailed afterbodies.

The research studies conducted so far have mostly focused on investigating the effect of a separate afterbody configuration on the drag reduction magnitude and the main research method is through experiments. In addition, the research objects of these studies are of different calibers and shapes; hence, it is impossible to summarize and generalize the obtained results. Moreover, of all components of the aerodynamic drag coefficient, the zero-lift drag coefficient is the most interesting parameter to be studied. It indicates the drag that a flying body experiences when no lift is generated. This coefficient provides deep

insights into the efficiency and performance of the flying object. Therefore, the primary objective of this paper is to compare the zero-lift drag reduction effectiveness of several most widely used afterbody configurations by determining the drags of projectiles with the same caliber and the same forebody configurations using the modern numerical simulation technique.

Computational methodology

Computational geometry

In this paper, five Army-Navy Spinner Rocket (ANSR) models with different afterbody configurations were evaluated on drag reduction effectiveness. These ANSR models with the corresponding afterbodies are presented in Figure 1, including the baseline, conical boattail, base cavity, multi-step, and a combination of conical boattail and base cavity afterbodies.

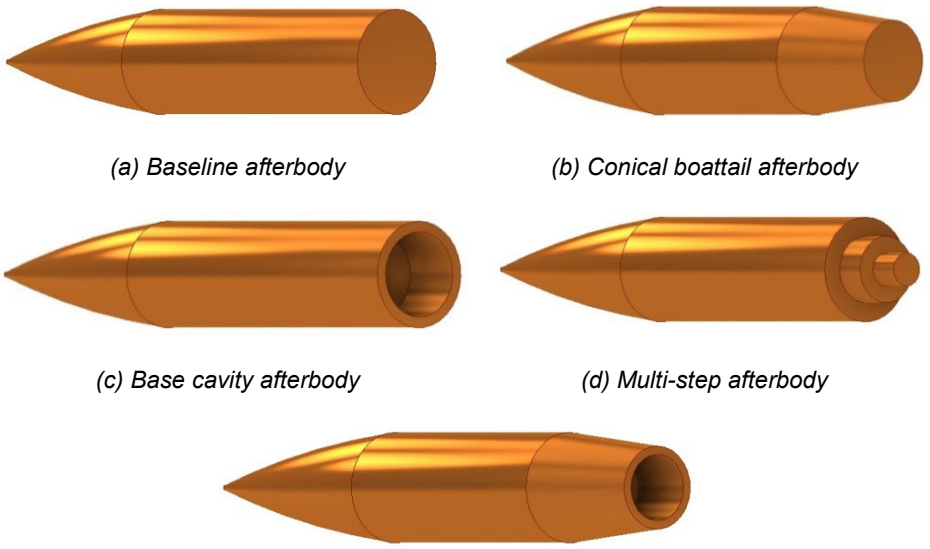

(a) Baseline afterbody

(b) Conical boattail afterbody

(c) Base cavity afterbody

(d) Multi-step afterbody

(e) Combination of a boattail and a base cavity

Figure 1 - Different ANSR afterbody configurations: (a) baseline afterbody; (b) conical boattail afterbody; (c) base cavity afterbody; (d) multi-step afterbody; and (e) conical boattail + base cavity afterbody

These configurations have the same total length of 5 calibers (1 caliber is 20mm) and the same 2-caliber secant ogive nose followed by a cylindrical bearing part of different length. The first configuration has the most simple afterbody and is used for baseline configuration. The second afterbody configuration consists of a conical boattail of 1-caliber length and a 7^0

inclination angle (Figure 2). The third afterbody configuration is a cylindrical base cavity with 0.8-caliber diameter and 1-caliber height. The fourth afterbody configuration consists of two steps with the same 0.5-caliber height; the first step diameter is 1/3-caliber and the second step diameter is 2/3-caliber. The fifth afterbody configuration is a combination of the second configuration with a cylindrical base cavity of 0.6-caliber diameter and 1-caliber height.

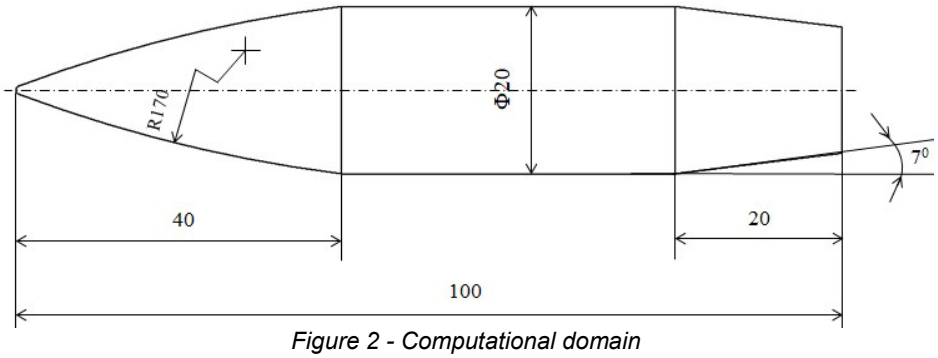

Figure 2 - Computational domain

Computational domain

Computational domains with the same dimensions were created for all model configurations in a cuboid form with 40L of length, 10L of width, and 10L of height (L is the total length of the computational model). This computational domain was created with dimensions large enough to accurately capture the aerodynamic phenomena taking place at the boundary layer and in the wake region behind the projectile base. The computational model was placed on the symmetrical longitudinal axis of the fluid domain and was 15L and 24L away from the Inlet and Outlet boundary respectively, as displayed in Figure 3.

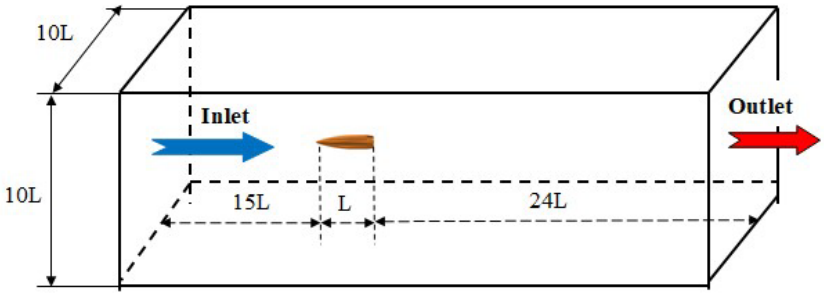

Figure 3 - Computational domain

Turbulence model

In order to simulate the flow around the models investigated in this work, the SST k-ω turbulence model were adopted. This is a two-equation eddy-viscosity turbulence model developed and improved by Menter (1994). This turbulence model blends the Standard *k-ε* and the Standard *k-ω* models to combine their advantages for enhancing the simulation accuracy and robustness. Near the wall region, it behaves like the *k-ω* model. In the free-stream region, it transitions to the *k-ε* model. This model provides more accurate predictions of flow separation than most RANS models and shows good performance in regions with adverse pressure gradients (Menter, 1994; Ameri et al., 2019). The two transport equations of the SST k-ω turbulence model are defined as follows (Menter, 1994):

$$\frac{\partial}{\partial t}(\rho k)+\frac{\partial}{\partial x_i}(\rho k u_i)=\frac{\partial}{\partial x_j}\left(\Gamma_k \frac{\partial k}{\partial x_j}\right)+G_k-Y_k+S_k, \tag{1}$$

$$\frac{\partial}{\partial t}(\rho \omega)+\frac{\partial}{\partial x_i}(\rho \omega u_i)=\frac{\partial}{\partial x_j}\left(\Gamma_\omega \frac{\partial \omega}{\partial x_j}\right)+G_\omega-Y_\omega+D_\omega+S_\omega, \tag{2}$$

where G_k is the turbulence kinetic energy due to the mean velocity gradients; G_ω is the generation of ω; Γ_k and Γ_ω are, respectively, the effective diffusivity of k and ω; Y_k and Y_ω are, respectively, the dissipations of k and ω due to the turbulence; S_k and S_ω are the user-defined source terms; D_ω is the the cross-diffusion term; and D_ω is the cross-diffusion term. The turbulent viscosity μ_t is defined as follows:

$$\mu_t=\frac{\rho k}{\omega}\frac{1}{max\left[1/\alpha^*, SF_2/\alpha_1\omega\right]}, \tag{3}$$

where α_1 is a constant of the turbulence model, S is the strain rate magnitude, and F_2 is a blending function. In the SST k-ω model, the turbulent Prandtl numbers σ_k and σ_ω are given as:

$$\sigma_k=\frac{1}{\frac{F_1}{\sigma_{k,1}}+\frac{1-F_1}{\sigma_{k,2}}},\ \sigma_\omega=\frac{1}{\frac{F_1}{\sigma_{\omega,1}}+\frac{1-F_1}{\sigma_{\omega,2}}}, \tag{4}$$

where F_1 is a blending function and $\sigma_{k,1}$, $\sigma_{k,2}$, $\sigma_{\omega,1}$, and $\sigma_{\omega,2}$ are constants.

The parameters G_k and G_ω are defined as:

$$G_k = min\left(G_k, 10\rho\beta^* k\omega\right),\ G_\omega = \frac{\alpha}{\upsilon_t} G_k, \tag{5}$$

The cross-diffusion term D_ω is determined as follows:

$$D_\omega = 2\left(1 - F_1\right)\rho\sigma_{\omega,2}\frac{1}{\omega}\frac{\partial k}{\partial x_j}\frac{\partial \omega}{\partial x_j}. \tag{6}$$

The model constants are given as follows: $\sigma_{k,1}$ = 1.176, $\sigma_{\omega,1}$ = 2.0, $\sigma_{k,2}$ = 1.0, $\sigma_{\omega,2}$ = 1.168, $\beta_{i,1}$ = 0.075, $\beta_{i,2}$ = 0.0828, β^* = 0.09, k = 0.41.

Solver and setup

In this study, the commercially available CFD software Ansys Fluent 2021 was used to evaluate the drag reduction of each afterbody configuration. A pressure-based solver with the Couple algorithm was chosen due to its robustness and accuracy. The air was set as an ideal gas. For the air viscosity model, the three-component Sutherland model were selected. The Inlet flow was defined as the Pressure far field and the Outlet flow was set as the Pressure outlet. On the body surface, the stationary, adiabatic and no-slip conditions were imposed. According to the ICAO atmosphere, the conditions for the atmosphere parameters were defined as follows: p_0 = 101325*Pa* and T_0 = 288.16*K* (ICAO, 1993). The simulations were considered converged once the flow residuals had reduced at least 5 orders in magnitude and the drag coefficient varied less than 1% over the last 100 iterations.

Mesh sensitivity study and result validation

It is well known that meshing is one of the factors affecting the simulation results. In this paper, a mesh sensitivity study was conducted to ensure the independence of the simulation results from the mesh resolutions. Firstly, the mesh sensitivity study was performed for the configuration with the baseline afterbody. To do that, six unstructured meshes with different resolutions were created by adjusting the size of the elements on the model surface as well as in the fluid domain to gradually refine the mesh while maintaining the dimensionless distance y+ less than 1 along the way. Numerical simulations were performed at the Mach number of 1.5 with the zero angle of attack under the same boundary conditions and the solver setup as presented above. The effect of the mesh resolutions on the simulated drag coefficient was presented in Table 1 and Figure 4.

Table 1 - Influence of the mesh resolutions on the simulation results

Mesh	Number of cells (x10^6)	C_{D0}	Deviation from the result of the previous mesh (%)
Mesh 1	0.734	0.536	-
Mesh 2	1.508	0.471	12.13
Mesh 3	2.492	0.422	10.40
Mesh 4	4.901	0.405	4.03
Mesh 5	7.553	0.404	0.25
Mesh 6	11.672	0.404	0

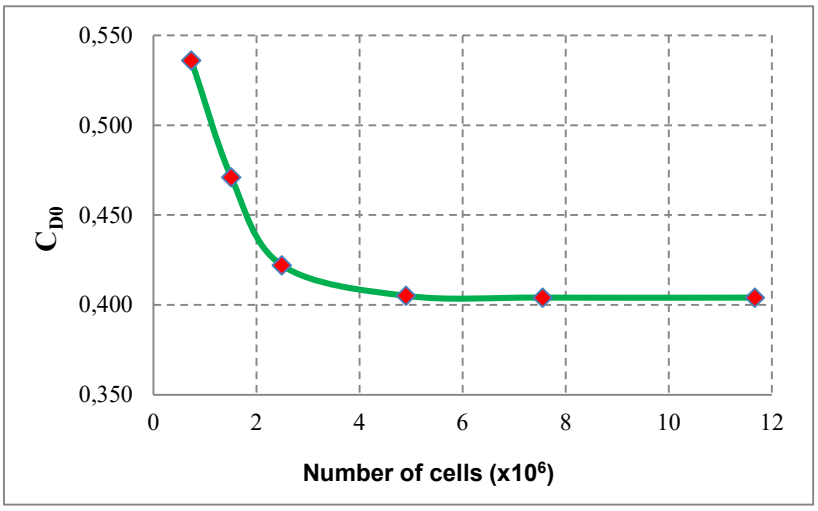

Figure 4 - Effect of the mesh resolutions on the total drag coefficient

Clearly, from the mesh size of 7.553 million of cells (Mesh 5), the subsequent mesh refinement practically will not affect the simulation results. For that reason, Mesh 5 was applied in this study for the ANSR baseline configuration taking into account a compromise between good accuracy and reasonable computation time. The adopted mesh was the finest on the projectile surface with the maximum cell size of 0.25mm and gets coarser from the region near the projectile surface to the fluid boundaries with the maximum cell size of 5mm. In order to maintain the dimensionless distance y+ less than 1, an additional 15-layer inflation with the first cell height of $5x10^{-4}$mm and a growth rate of 1.15 was added for better capturing the aerodynamics phenomena taking place in the vicinity of the projectile surface

and in the region directly behind the projectile base. The mesh structure used for the ANSR baseline afterbody configuration in this research is shown in Figure 5.

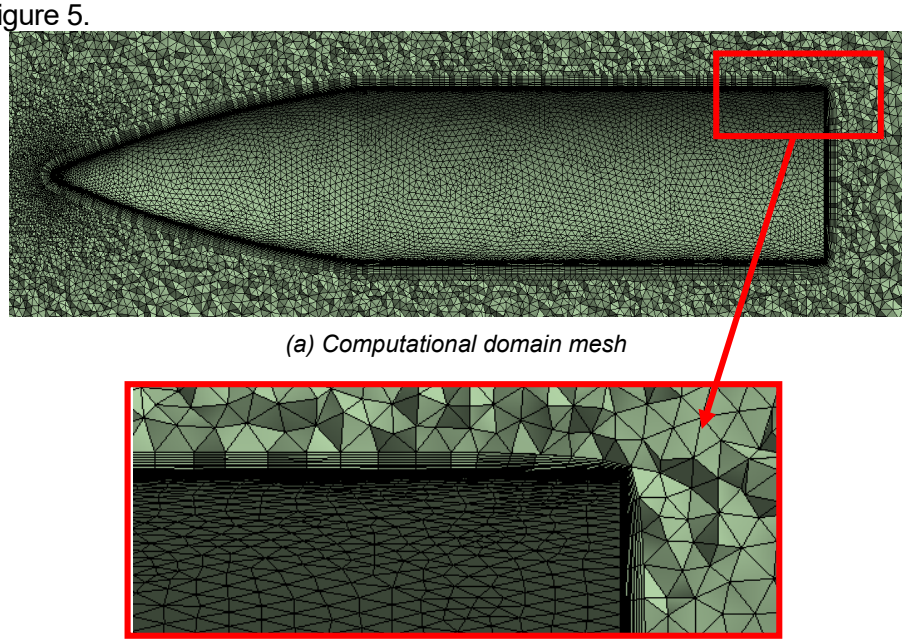

(a) Computational domain mesh

(b) A close-up view of the refined mesh near the afterbody surface

Figure 5 - Unstructured mesh used for the ANSR baseline configuration: (a) computational domain mesh; (b) a close-up view of the refined mesh near the afterbody surface

Next, the meshes for the remaining ANSR configurations were created based on the mesh structure used for the baseline ANSR after conducting an additional mesh sensitivity study for each case. Specifically, two meshes were created for each remaining ANSR configuration: the first mesh is based on the mesh configuration used for the baseline ANSR, while the second mesh has twice as many cells as the first mesh. The numerical simulations were then performed for these two meshes. In all cases, the numerical simulations have shown the same results. This has indicated that there is no need for further refinement of the meshes. Therefore, the meshes created for the remaining ANSR configurations based on the mesh structure used for the baseline ANSR were employed in this study. As a result, the meshes for the ANSRs with a conical boattail afterbody, a base cavity afterbody, a multi-step afterbody, and a combination of a conical boattail and a base cavity afterbody consist of 7.281, 7.781, 7.207 and 7.341 million of cells, respectively. The

close-up views of the meshes near the surface of the computational models for each ANSR configuration are displayed in Figure 6.

Eventually, the simulated total drag coefficient of the ANSR with a baseline afterbody was employed to validate the adopted computational methodology. The total drag coefficient obtained for the ANSR with a baseline afterbody through numerical simulation at the Mach number of 1.5 is 0.404, while the corresponding value obtained by Platou (1975) through experiments is 0.409. The relative deviation is only 1.22% demonstrating that the created meshes can be used with high confidence in this study.

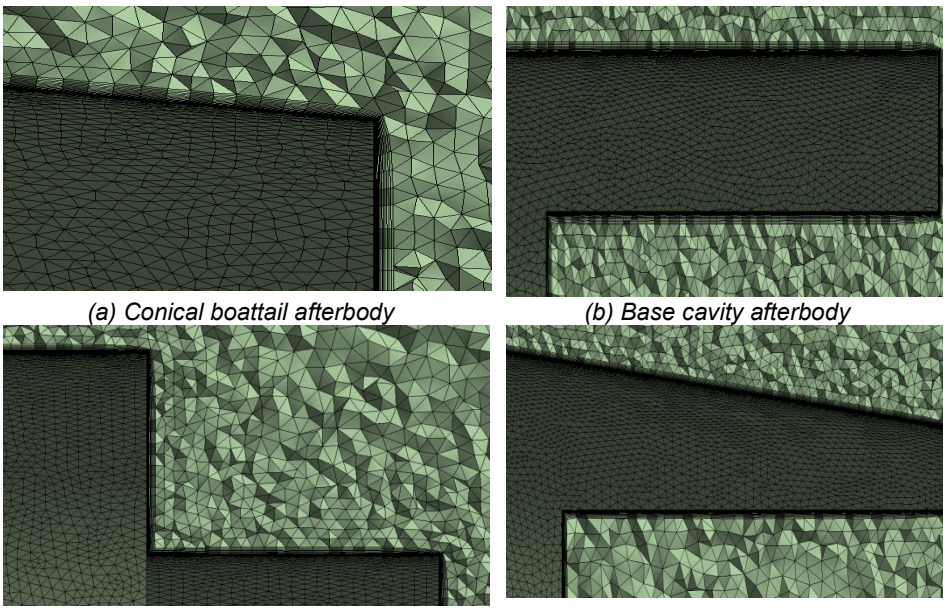

(a) Conical boattail afterbody *(b) Base cavity afterbody*

(c) Multi-step afterbody *(d) Boattail + Base cavity afterbody*

Figure 6 - Close-up views of the refined mesh near the afterbody surface:

a) conical boattail (top left); b) vase cavity afterbody (top right); c) multi-step afterbody (bottom left); and d) boattail + Base cavity (bottom right)

Results and discussion

Drag reduction effectiveness of different afterbody configurations

In this paper, to evaluate the drag reduction effectiveness of afterbody configurations at supersonic speeds, numerical simulations

were carried out for each configuration at Mach numbers ranging from 1.5 to 4.0 with an increment of 0.5. The obtained total drag coefficients C_{D0} are listed in Table 2. The relative drag reduction of each configuration compared to the baseline configuration was also calculated and presented in Table 2.

Based on the obtained results, several remarks can be derived. First of all, if not taking into account the combination of a conical boattail and a base cavity, then the conical boattail is the most effective configuration for drag reduction showing a drag reduction of up to 12.46% and the average drag reduction of the conical boattail configuration is 10.99% for the Mach number interval from 1.5 to 4.0. Meanwhile, the base cavity afterbody seems to be the least effective configuration with the maximum drag reduction of only 1.73% and the average drag reduction for the entire Mach number interval is 1.33%. However, adding a base cavity to the conical boattail configuration can provide additional drag reduction with the maximum drag reduction of up to 13.48%. Although the multi-step configuration is a better alternative for drag reduction than the base cavity configuration, the drag reduction provided by this configuration is still small compared to the conical boattail configuration. Overall, the multi-step configuration can provide a total drag reduction of 2.15% on the average. Generally speaking, the most effective afterbody configuration in terms of total drag reduction is the combination of a conical boattail and a base cavity showing an average drag reduction of 11.96%. The second most effective configuration is the conical boattail providing a total drag reduction of 10.99% on the average. Additionally, the least effective configuration is the base cavity afterbody with the average drag reduction of only 1.33%.

The results obtained in this study have shown a very good agreement with other simulations. Namely, Suliman et al. (2009) pointed out that for a 155mm M549 artillery shell, the case of using a base cavity alone has shown the smallest reduction in the drag coefficient of only 1-2%, while having a boattail afterbody can reduce the total drag coefficient by about 12%. An experimental investigation conducted by Kidd et al. (1990) for a spin-stabilized and a fin- stabilized projectiles also revealed that the multi-stepped afterbody does not

significantly reduce the total drag at supersonic flight regimes compared to the flat baseline afterbody.

Table 2 - Total drag coefficient and relative drag reduction for different afterbody configurations

	Total drag coefficient C_{D0}					Drag reduction compared to the baseline configuration (%)			
M	Baseline	Conical boattail	Base Cavity	Multi-step	Boattail + Cavity	Conical boattail	Base Cavity	Multi-step	Boattail + Cavity
1.5	0.404	0.355	0.397	0.391	0.351	12.13	1.73	3.22	13.12
2.0	0.356	0.312	0.351	0.347	0.308	12.36	1.40	2.53	13.48
2.5	0.313	0.274	0.309	0.307	0.271	12.46	1.28	1.92	13.42
3.0	0.275	0.245	0.271	0.270	0.242	10.91	1.45	1.82	12.00
3.5	0.243	0.220	0.240	0.238	0.217	9.47	1.23	2.06	10.70
4.0	0.221	0.202	0.219	0.218	0.201	8.60	0.90	1.36	9.05
Average						10.99	1.33	2.15	11.96

The total drag coefficients obtained for each afterbody configuration as functions of the Mach number are presented in Figure 7. Obviously, the curves of the total drag coefficients follow the same fluctuation trend showing a constant decrease with the increase in Mach numbers. The curve of the baseline configuration is the highest followed by the curves of the base cavity and the multi-step configurations. The lowest curves are those of the conical boattail and the combined configurations. However, the curves of the base cavity and the multi-step configurations are situated very close to the curve of the baseline configuration. That means the drag reductions provided by these two afterbody configurations are insubstantial. Conversely, the curves of the conical boattail and the combined configurations located far below the curve of the baseline configuration show a significant drag reduction for all Mach numbers of interest.

Apart from the total drag coefficients, it is interesting to see how the base drag changes in each case of configurations. The base drag coefficients C_{DB} of the investigated afterbody configurations as functions of the Mach number are presented in Figure 8.

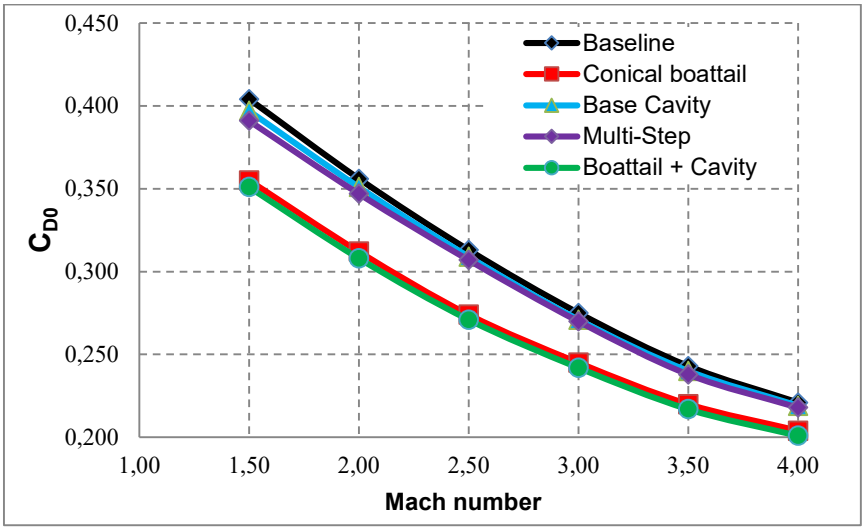

Figure 7 - Total drag coefficient for different afterbody configurations versus Mach

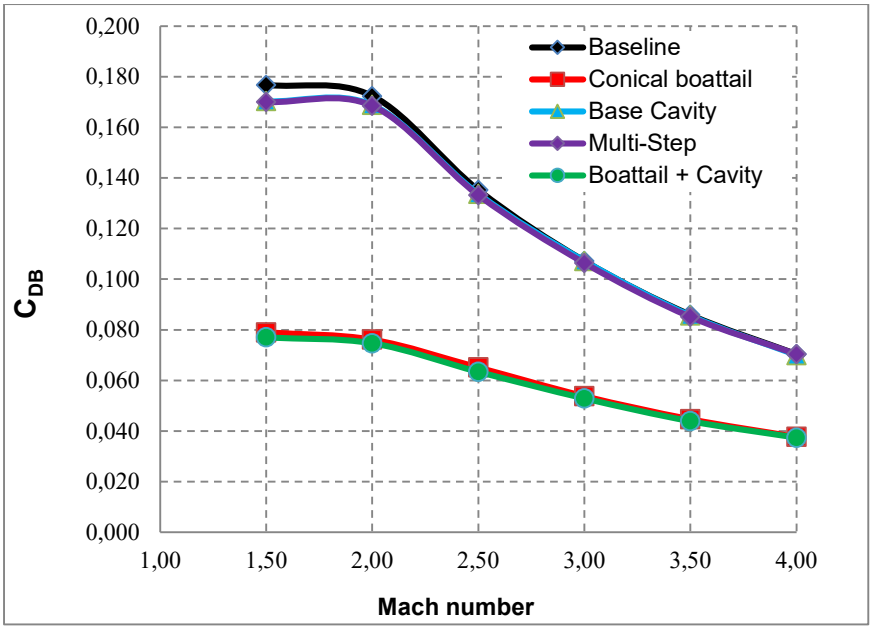

Figure 8 - Base drag coefficient for different afterbody configurations versus Mach

Clearly, as in the case of the total drag coefficients, the base drag coefficients of the studied configurations also follow the same

fluctuation trend. The relative positions between the curves of the base drag coefficients follow the same manner as the curves of the total drag coefficients. The conical boattail configuration and the combined configuration provide the most significant reduction in base drag. The base cavity configuration and the multi-step configurations are the least effective for base drag reduction for the entire interval of the Mach numbers of interest.

Flow field visualization

One of the main advantages of numerical simulation methods is the ability to visualize the flow field around a flying object. In this study, the flow Mach number profiles obtained at Mach 2.0 are presented in Figures 9 to 13.

The presence of the phenomena such as normal and oblique shock waves which characterize the supersonic flow regime can be clearly seen in all cases. Moreover, the flow separation takes place at the projectile base edge leading to the formation of a recirculation flow behind the projectile base. However, the near-wake regions for the conical boattail and the combined configurations are significantly smaller than those of the remaining configurations. That flow behavior has led to a significant change in the pressure distribution on the projectile base surface resulting in appreciable total drag reduction as expected.

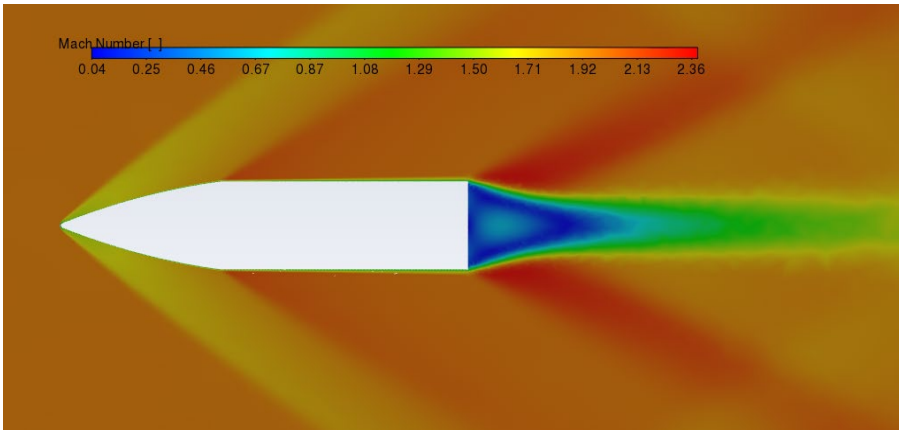

Figure 9 – Mach number profile around the projectile with the baseline afterbody at Mach 2.0

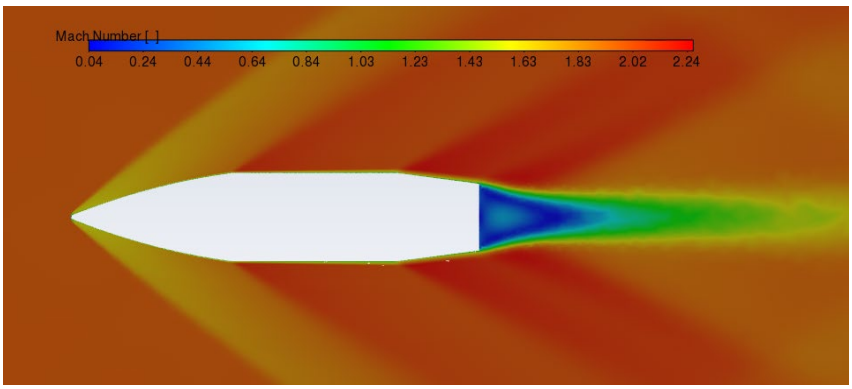

Figure 10 - Mach number profile around the projectile with the conical boattail afterbody at Mach 2.0

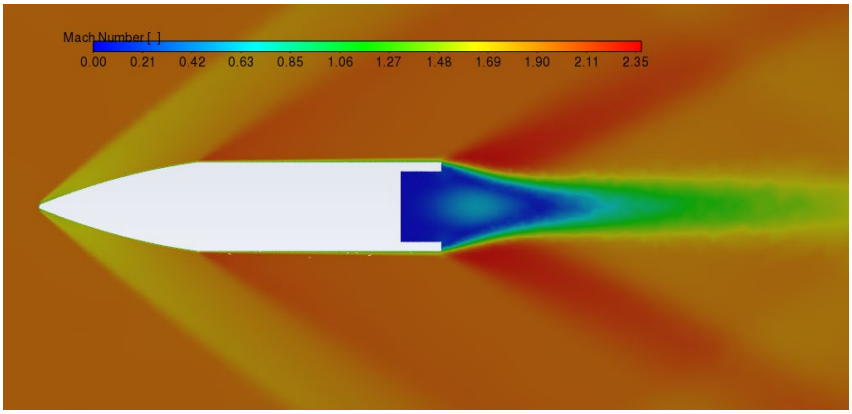

Figure 11 - Mach number profile around the projectile with the base cavity afterbody at Mach 2.0

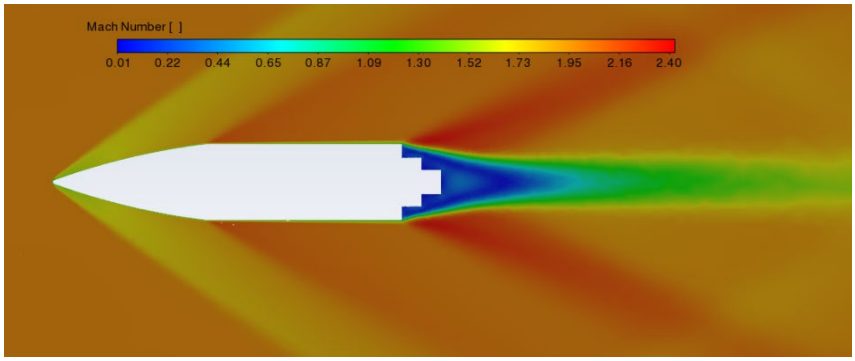

Figure 12 - Mach number profile around the projectile with the multi-step afterbody at Mach 2.0

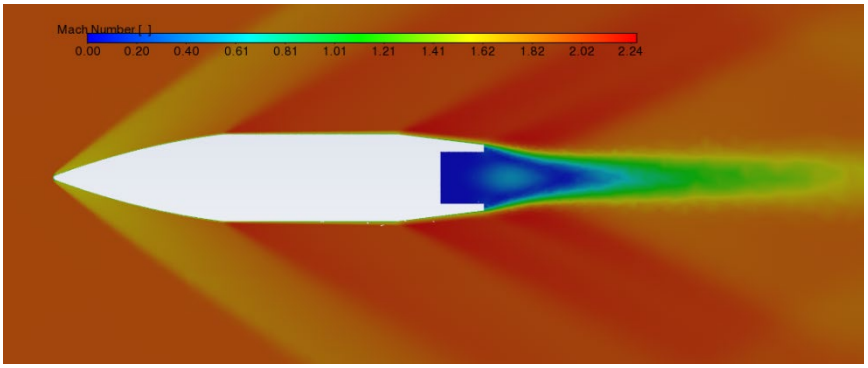

Figure 13 - Mach number profile around the projectile with a combination of the conical boattail and the base cavity at Mach 2.0

Conclusion

In this paper, numerical simulations were performed for ANSRs with five different afterbody configurations to investigate their effect on the aerodynamics and flow structure around the afterbody region. Based on the research results, several important insights can be gained. Firstly, the conical boattail afterbody is the most effective passive device to lower the total drag acting on the projectile, reducing it by up to 12.46 % of the total drag. A combination of the conical boattail and a base cavity can potentially reduce the total drag coefficient by up to 13.48%. For the 5-caliber ANSR, a base cavity alone as well as a multi-step afterbody alone can reduce the total drag coefficient but not significantly, by 1.33% and 2.15%, respectively. These simulation results agree well with other experimental and simulation data for larger caliber projectiles. Secondly, the afterbody modifications greatly affect the structure of the flow field around the projectile base, changing the recirculation region and the base pressure. The findings of this research are significant contributions to a better understanding of the effectiveness of different passive drag reduction devices for small caliber spinning projectiles in particular, and to a broadening knowledge about aerodynamics of slender bodies in general. The results obtained in the present study can be applied for selecting appropriate means for drag reduction of small caliber projectiles.

Future work

The presented study has clarified certain questions about the performance of different afterbody configurations regarding the zero-lift drag reduction of a small caliber projectile. However, further works need

to be done to quantify their efficiency of drag reduction with a varying angle of attack, as well as to evaluate their effect on the dynamic characteristics, namely, roll damping moment, pitch damping moment, and Magnus force and moment to assess their overall aerodynamic performance. Therefore, further analysis of the aerodynamic performance of these afterbody configurations would be recommended for a deeper understanding of effects that each of them have on the general aerodynamic performance of a projectile.

References

Ameri, M.J., Heidari, M.R., Nowruzi, H. & Najafi, A. 2019. Analysis of different turbulence models in simulation of hypersonic flow in the wind tunnel. *American Journal of Mechanical Engineering*, 7(4), pp. 172-180. Available at: http://pubs.sciepub.com/ajme/7/4/3 [Accessed: 22 January 2025].

El-Awwad, E., Ibrahim, A.Z., El-Sebae, A.M. & Riad, A.M. 2020. Flow computations past a triangular boattailed projectile. *Defence Technology*, 16(3), pp. 712-719. Available at: https://doi.org/10.1016/j.dt.2019.08.009

Fu, J. & Liang, S. A. 1994. Numerical study of optimal drag reduction for turbulent transonic projectiles using a passive control. *International Journal of Computational Fluid Dynamics*, 3(3-4), pp. 251-264. Available at: https://doi.org/10.1080/10618569408904510

Guidos, B. & Sturek, W. 1987. *Computational aerodynamic analysis for a range-limited 25mm training round*. US Army Ballistic Research Laboratory, Aberdeen Proving Ground, Maryland, Technical Report BRL-TR-2833. Available at: https://apps.dtic.mil/sti/citations/ADA185270 [Accessed: 22 January 2025].

ICAO. 1993. *Manual of the ICAO standard atmosphere extended to 80 kilometres (262 500 feet). International Civil Aviation Organization, Doc 7488/3*. Available at: https://aiac.ma/wp-content/uploads/2018/01/Manuel-de-l%E2%80%99atmosph%C3%A8re-Type-OACI-Doc7488-1.pdf [Accessed: 22 January 2025].

Ibrahim, A. & Filippone, A. 2010. Supersonic aerodynamics of a projectile with slot cavities. *The Aeronautical Journal*, 114(1151), pp. 15-24. Available at: https://doi.org/10.1017/S0001924000003493

Kidd, J.A., Wikoff, D. & Cottrell, C. J. 1990. Drag reduction by controlling flow separation using stepped afterbodies. *Journal of Aircraft*, *27*(6), pp. 564-566. Available at: https://doi.org/10.2514/3.25320

Kumar, A., Panda, H.S., Biswal, T.K. & Appavuraj, R. 2014. Flow around a conical nose with rounded tail projectile for subsonic, transonic, and supersonic flow regimes: A numerical study. *Defence Science Journal*, 64(6), pp. 509-516. Available at: https://doi.org/10.14429/dsj.64.8111

Lu, H. & Zhang, Q. 2022. Numerical investigation on aerodynamic drag reducing of slender body with non-cylindrical base cavity. In: *Proceedings of the*

2022 International Conference on Smart Manufacturing and Material Processing, pp. 227-234. Available at: https://doi.org/10.3233/ATDE220838

Lunghi, G., Pasqualetto, E., Mariotti, A. & Salvetti, M.V. 2024. Drag reduction in a spanwise-infinite boat-tailed body through multiple transverse grooves. *Computers & Fluids*, *275*, 106250. Available at: https://doi.org/10.1016/j.compfluid.2024.106250

Ma, J., Chen, Z., Xue, D. & Sun, X. 2020. Influences of boattail structures on aerodynamic characteristics of supersonic spinning projectiles. *Theoretical and Computational Fluid Dynamics*, 34, pp. 249-270. Available at: https://doi.org/10.1007/s00162-020-00532-0

Mahdi, A.S. & Al-Atabi, M. 2008. Effect of body shape on the aerodynamics of projectiles at supersonic speeds. *Journal of Engineering Science and Technology*, 3(3), pp .278-292. Available at: https://jestec.taylors.edu.my/Vol%203%20Issue%203%20December%2008/Vol_3_3_278-292_abdulkareem_mushtak.pdf [Accessed: 22 January 2025].

Mariotti, A., Buresti, G., Gaggini, G. & Salvetti, M.V. 2017. Separation control and drag reduction for boat-tailed axisymmetric bodies through contoured transverse grooves. *Journal of Fluid Mechanics*, 832, pp. 514-549. Available at: https://doi.org/10.1017/jfm.2017.676

Mathur, N.B. & Viswanath, P.R. 2004. Drag reduction from square base afterbodies at high speeds. *Journal of aircraft*, 41(4), pp. 811-820. Available at: https://doi.org/10.2514/1.532

Menter, F.R. 1994. Two-equation eddy-viscosity turbulence models for engineering applications. *AIAA Journal*, 32(8), pp. 1598-1605. Available at: https://doi.org/10.2514/3.12149

Platou, A.S. 1975. Improved projectile boattail. *Journal of Spacecraft and Rockets*, 12(12), pp. 727-732. Available at: https://doi.org/10.2514/3.57040

Suliman, M.A., Mahmoud, O.K., Al-Sanabawy, M.A. & Abdel-Hamid, O. E. 2009. Computational investigation of base drag reduction for a projectile at different flight regimes. In: *International Conference on Aerospace Sciences and Aviation Technology*, 13, No. Aerospace sciences & Aviation technology, ASAT-13, pp. 1-13. The Military Technical College. Available at: https://www.researchgate.net/publication/298353323_Computational_investigation_of_base_drag_reduction_for_a_projectile_at_different_flight_regimes [Accessed: 22 January 2025].

Viswanath, P.R. 2001. Drag reduction of afterbodies by controlled separated flows. *Journal of aircraft*, 39(1), pp. 73-78. Available at: https://doi.org/10.2514/2.1272

Viswanath, P.R. & Patil, S.R. 1990. Effectiveness of passive devices for axisymmetric base drag reduction at Mach 2. *Journal of Spacecraft and Rockets*, 27(3), pp. 234-237. Available at: https://doi.org/10.2514/3.26130

Viswanath, P.R. & Patil, S.R. 1997. Zero-lift drag characteristics of afterbodies with a square base. *Journal of spacecraft and rockets*, 34(3), pp.290-293. Available at: https://doi.org/10.2514/2.3231

Рачунарска студија о ефикасности смањења отпора ротирајућих пројектила са различитим конфигурацијама задњег тела при суперсоничним брзинама

Кван Туан Нуиен, **аутор за преписку**

Државни технички универзитет „Ле Куи Дон", Факултет специјалног машинства, Ханој, Социјалистичка Република Вијетнам

ОБЛАСТ: машинство, динамика флуида
КАТЕГОРИЈА (ТИП) ЧЛАНКА: оригинални научни рад

Сажетак:

Увод/циљ: У овом раду нумерички је процењена ефикасност смањења отпора при надзвучним брзинама пет конфигурација са различитим задњим телом ракета „спинер" које поседује војска и морнарица.

Методе: Једначине Реинолдс-Аверагед Навиер-Стокес са SST к-ω моделом турбуленције коришћене су за нумеричке симулације. Студије осетљивости мреже предузете су како би се осигурала независност резултата симулације од величине мреже. Резултати симулације су потврђени на основу архивских експерименталних података. Извршено је поређење коефицијената аеродинамичког отпора за основну линију и модификована задња тела. Визуализована су и анализирана поља струјања око различитих конфигурација накнадног тела.

Резултати: Резултати истраживања су показали да су конусни чамац или комбинација конусног чамца са базном шупљином најефикасније методе које показују у просеку 10,99%, односно 11,96% смањење отпора. Сама конфигурација базне шупљине је најмање ефикасан метод који показује просечно смањење отпора од само 1,33% у поређењу са основном конфигурацијом. Вишестепена конфигурација накнадног тела може да оствари просечно смањење отпора од 2,15% у поређењу са основном конфигурацијом.

Закључак: Конфигурације задњег тела знатно утичу на аеродинамички отпор пројектила који се окреће. Од разматраних конфигурација задњег тела комбинација конусног репа и базне шупљине је најефикаснији начин да се смањи отпор пројектила. Налази представљени у овој студији пружили су значајан увид у боље разумевање пасивних метода за смањење аеродинамичког отпора.

Кључне речи: нумеричка симулација, аеродинамичке карактеристике, смањење отпора, конусни боатаил, базна шупљина.

Nguyen, Q. T. , A computational study on the drag reduction effectiveness of a spinning projectile with different afterbody configurations at supersonic speeds. pp.1307-1326

Paper received on: 22.03.2025.
Manuscript corrections submitted on:11.04.2025.
Paper accepted for publishing on: 27.05.2025.